Two-dimensional metallic behavior at polar $MgO/BaTiO_3$ (110) interfaces*

Du Yan-Ling(杜颜伶)[a)b)], Wang Chun-Lei(王春雷)[a)], Li Ji-Chao(李吉超)[a)†],
Zhang Xin-Hua(张新华)[a)], Wang Fu-Ning(王芙凝)[a)], Liu Jian(刘 剑)[a)],
Zhu Yuan-Hu(祝元虎)[a)], Yin Na(尹 娜)[a)], and Mei Liang-Mo(梅良模)[a)]

[a)] *School of Physics, Shandong University, Jinan* 250100, *China*
[b)] *College of Science and Technology, Shandong University of Traditional Chinese Medicine, Jinan* 250355, *China*

(Received 22 August 2014; revised manuscript received 5 October 2014; published online 30 January 2015)

The first-principles calculations are employed to investigate the electrical properties of polar $MgO/BaTiO_3$ (110) interfaces. Both n-type and p-type polar interfaces show a two-dimensional metallic behavior. For the n-type polar interface, the interface Ti 3d electrons are the origin of the metallic and magnetic properties. Varying the thickness of $BaTiO_3$ may induce an insulator–metal transition, and the critical thickness is 4 unit cells. For the p-type polar interface, holes preferentially occupy the interface O $2p_y$ state, resulting in a conducting interface. The unbalance of the spin splitting of the O 2p states in the interface MgO layer leads to a magnetic moment of about $0.25\mu_B$ per O atom at the interface. These results further demonstrate that other polar interfaces, besides $LaAlO_3/SrTiO_3$, can show a two-dimensional metallic behavior. It is helpful to fully understand the role of polar discontinuity on the properties of the interface, which widens the field of polar-nonpolar interfaces.

Keywords: electronic structures, $MgO/BaTiO_3$ (110) polar interfaces, two-dimensional electron gas (2DEG), magnetism

PACS: 73.20.At, 75.70.Cn, 73.20.–r, 75.70.–i **DOI:** 10.1088/1674-1056/24/3/037301

1. Introduction

Since a high-mobility electron gas was discovered at the $LaAlO_3/SrTiO_3$ interface,[1] much effort has been devoted to reveal its origin. Many researchers have investigated the roles of many factors, including oxygen vacancies,[2,3] chemical intermixing,[4] the thickness of the $LaAlO_3$ sheets,[5,6] the external electric field,[7–9] and the epitaxial strain.[10] Besides them, the polarity discontinuity at the interface has been considered to be the dominant mechanism behind the phenomenon.[1,11–15] In $LaAlO_3/SrTiO_3$(001) heterostructures, the atomic layers in $SrTiO_3$ are nominally charge neutral, whereas the atomic layers in $LaAlO_3$ can be represented by alternating $(LaO)^+$ and $(AlO_2)^-$ layers in principle. Therefore, a polar discontinuity is expected at the interface between $SrTiO_3$ and $LaAlO_3$. In order to stabilize this discontinuity, it has been suggested that an extra 0.5 electron per two-dimensional unit cell is transferred from $LaAlO_3$ ($SrTiO_3$) to $SrTiO_3$ ($LaAlO_3$) in the n (p)-type interface. This model has been supported by atomic-scale electron energy-loss spectroscopy (EELS) measurements, which show that the n-type interface can be realized by the mixed valency of Ti, whereas the p-type interface can be realized by oxygen vacancies.[16]

In order to examine whether the role of the polar discontinuity at the interface is general, or unique to the $LaAlO_3/SrTiO_3$ interface, researchers have grown other superlattices with a mismatch between polar and nonpolar layers.[17–19] Hotta and his cooperator[17] investigated the transport properties of $LaVO_3/SrTiO_3$ heterointerfaces, and found that the n-type $VO_2/LaO/TiO_2$ interface is conducting, while the p-type $VO_2/SrO/TiO_2$ interface is insulating, similar to that in $LaAlO_3/SrTiO_3$. Wang *et al.*[18] studied the $LaAlO_3/EuO$(001) interface, and demonstrated that the mechanism responsible for the two-dimensional electron gas (2DEG) at the interface is similar to that for the $LaAlO_3/SrTiO_3$ interface. Perna *et al.*[19] investigated heterostructures based on a different overlayer. They replaced $LaAlO_3$ with $LaGaO_3$ and found a highly conductive interface. All the above results demonstrate that other polar interfaces, besides $LaAlO_3/SrTiO_3$, can be metallic and generate a 2DEG at the interfaces.

In this paper, we investigate the electronic structures of polar $MgO/BaTiO_3$ (110) interfaces, in which a nonperovskite MgO (110) film is adopted as a capping layer on the $BaTiO_3$ (110) substrate. Along the [110] direction, $BaTiO_3$ can be represented by planar stacks of $[BaTiO]^{4+}$ and $[O_2]^{4-}$ layers, while MgO is composed of neutral layers. Similar to the $LaAlO_3/SrTiO_3$ interface, the polar discontinuity at the $MgO/BaTiO_3$ (110) interface needs to be compensated by electron transfer. Thus, the $MgO/BaTiO_3$ (110) interface is expected to be conductive. As is well known, both

*Project supported by the National Basic Research Program of China (Grant No. 2013CB632506), the National Natural Science Foundation of China (Grant Nos. 11374186, 51231007, 51202132, and 51102153), and the Independent Innovation Foundation of Shandong University, China (Grant No. 2012TS027).

†Corresponding author. E-mail: lijichao@sdu.edu.cn

© 2015 Chinese Physical Society and IOP Publishing Ltd

MgO and $BaTiO_3$ are wide band-gap insulators. The rock-salt MgO has a lattice constant of 4.21 Å,[20] while the lattice constant of $BaTiO_3$ with the perovskite cubic structure is 4.00 Å,[21] so there is a little lattice mismatch between MgO and $BaTiO_3$. Due to its broad applications in capacitors[22] and electro-optical devices,[23,24] $BaTiO_3$/MgO (001) has attracted much attention, and been fabricated using magnetron sputtering,[25–27] chemical vapor deposition,[28] and pulsed laser deposition.[23,29] However, there are few studies about the polar MgO/$BaTiO_3$ (110) interfaces. Investigating the relaxation and electronic structures of the polar MgO/$BaTiO_3$ (110) interfaces not only is helpful to fully understand the role of the polarity discontinuity on the properties of the interface but also adds to the understanding of the MgO/$BaTiO_3$ interface.

2. Model and method

In this paper, a thin MgO film deposited on the $BaTiO_3$ (110) substrate is modeled by $(MgO)_8/(BaTiO_3)_5$ (110) heterostructures, containing 8 unit cells (four layers) of MgO and 5 unit cells of $BaTiO_3$ within the heterostructures. Along the [110] direction, $BaTiO_3$ can be represented by planar stacks of $[BaTiO]^{4+}$ and $[O_2]^{4-}$ layers, resulting in two types of terminations: O_2-termination and BaTiO-termination. In the case of MgO, it is composed of $[MgO]^0$ charge-neutral stacks along the [110] direction. Thus, two polar interfaces are possible: the n-type MgO/BaTiO interface and the p-type MgO/O_2 interface. As far as the thermodynamic stability is concerned, we choose the interface structure with the lowest energy. To model the MgO ultrathin film deposited on the $BaTiO_3$ substrate, atoms in the lowest two layers of the heterostructures are fixed, and other atoms fully relax. The in-plane lattice constants of the heterostructures are fixed to those of $BaTiO_3$. For cubic $BaTiO_3$, we obtain a lattice constant of 3.953 Å within LDA, which is very close to the experimental value of 4.00 Å[21] and other theoretical results of 3.951 Å[30] and 3.958 Å.[31] Thus, the in-plane lattice constants a and b of the heterostructures are fixed at 3.953 Å and 5.59 Å, respectively. For cubic MgO, we obtain a lattice constant of 4.15 Å within LDA, which is very close to the experimental value of 4.21 Å.[20,32] Thus, to modulate the thin layers of $BaTiO_3$ grown on the top of the MgO substrate, the in-plane lattice constants a and b of the heterostructures are fixed at 4.15 Å and 5.59 Å, respectively. A vacuum spacing of 10 Å between adjacent slabs is included in each of the heterostructures to minimize the interaction between neighboring surfaces.

In this work, the first-principles density functional calculations are performed using the Vienna *ab initio* simulation package (VASP).[33,34] The ion–electron interactions are described by using the projector augmented wave (PAW) method,[35] and the local density approximation (LDA) is used for the exchange–correlation energy of electrons.[36] Calculations are performed using a 5×4×1 Monkhorst–Pack[37] k-point mesh and a kinetic energy cutoff of 500 eV. The atoms except those in the lowest two layers are fully relaxed until the forces on the ions are less than 0.01 eV/Å.

3. Results and discussion

3.1. The n-type interface

We investigate the n-type MgO/BaTiO (110) interface in the $(MgO)_8/(BaTiO_3)_5$ heterostructures. Figure 1 shows the relaxed n-type MgO/BaTiO (110) interface. From the figure, we can see that the relaxation of the MgO slab is inconspicuous. Because the in-plane lattice constant of MgO is larger than that of $BaTiO_3$, the MgO slab is under compressive strain. It is expected that the lattice constant of the relaxed MgO slab along the [110] direction would be larger than that before relaxation. However, the change is not obvious, the lattice constant of MgO along the [110] direction becomes 1.04 times of that before relaxation. In contrast to the unconspicuous relaxation in the MgO slab, the displacements of atoms in the $BaTiO_3$ slab are significant: Ti and Ba atoms relax away from the interface, while O atoms relax close to the interface. A more thorough insight can be obtained by analyzing the relative displacements between M (M denotes Ba, Ti, or Mg) and O atoms, which are listed in Table 1. From the table, we can see that the relaxations of both Mg and O atoms in the surface MgO layer are similar, resulting in only a small

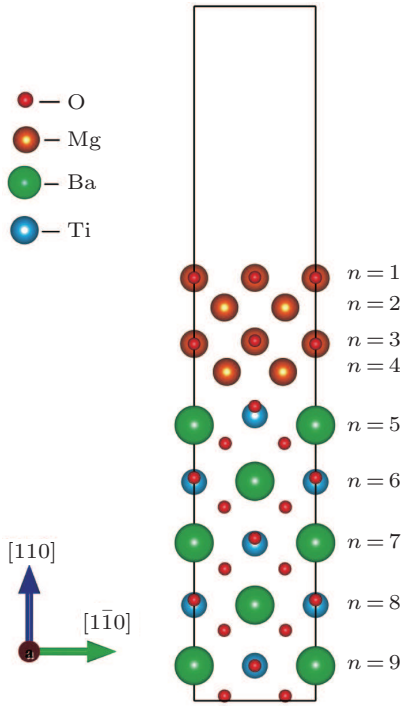


Fig. 1. (color online) Relaxed structure of the $(MgO)_8/(BaTiO_3)_5$ (110) heterostructure with an n-type $(MgO)^0/(BaTiO)^{4+}$ interface, containing 8 unit cells (four layers) of MgO and 5 unit cells of $BaTiO_3$ within the heterostructure. Index n denotes atomic monolayers and is increasing with the distance from the surface.

buckling of 0.03 Å. The largest structural relaxation occurs in the interface BaTiO layer, and the relative displacement between O and Ba atoms results in a big buckling of 0.60 Å. The relative displacement between O and Ti (Ba) ions results in a polarization $\boldsymbol{P}$ pointed away from the interface, which can reduce the built-in potential in the $BaTiO_3$ (110) slab[38] and the instability of the polar interface. In addition, the distortion of the Ti–O octahedrons can lead to the splitting of the Ti 3d obitals and the electronic reconstruction at the polar n-type MgO/BaTiO (110) interface.

Table 1. Relative displacements between relaxed M (M denotes Ba, Ti, or Mg) and O atoms, Δ (M–O). The relative displacement denotes the displacement of cations (Ba, Ti or Mg) minus that of O anions in each layer along the c axis.

Layer n	1	2	3	4	5	6	7	8	9
Δ (Ba–O)/Å	–	–	–	–	–0.60	–0.17	–0.22	–0.24	0.00
Δ (Ti–O)/Å	–	–	–	–	–0.42	–0.19	–0.26	–0.22	0.00
Δ (Mg–O)/Å	–0.03	0.10	0.03	0.16	–	–	–	–	–

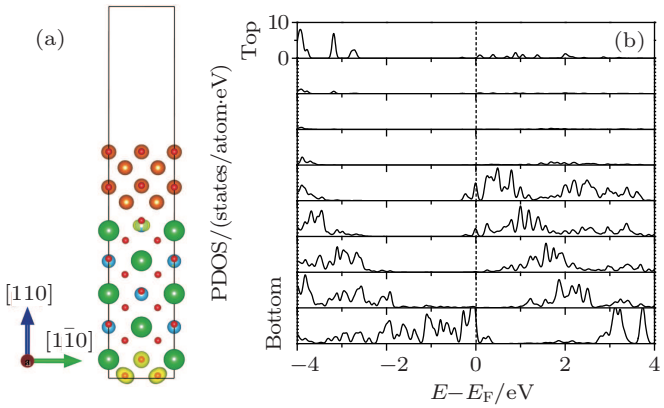


Fig. 2. (color online) (a) The 3D isovalue surface (yellow contour) of the local density of states contributing to the peak at the Fermi level. (b) The partial density of states grouped by layers of the $(MgO)_8/(BaTiO_3)_5$ (110) heterostructure with an n-type interface. The data (plot of a charge isosurface and PDOS) for each layer are aligned on the same vertical position. The Fermi level is highlighted by the black dashed line.

Electronic properties of the n-type MgO/BaTiO (110) interface are calculated by the LDA method, and shown in Fig. 2. Figure 2(a) is the plot of the 3D isovalue surface (yellow contour) of the local density of states contributing to the peak at the Fermi level, which describes the spatial distribution of transferred electrons and holes, respectively. From the figure, it can be observed that the holes are confined in the bottom layer, while the free electrons concentrate preferentially at the interfaces, resulting in a 2DEG formed at the interface BaTiO layer. In order to gain more insight into the spatial distribution of electronic states, the partial density of states grouped by layers of the heterostructure is shown in Fig. 2(b). From the figure, we can see that there is a band-bending in the partial density of states. The bottom of the conduction band is determined by the Ti $3d_{xy}$ band at the interface BaTiO layer, while the top of the valence band is fixed by the O 2p band in the bottom layer. Thus, the closing of the gap is due to the reducing of the interface Ti $3d_{xy}$ band states at the interface BaTiO layer as the $BaTiO_3$ slab gets thicker. With the interface Ti $3d_{xy}$ electrons dipping below the Fermi level, a 2DEG emerges at the interface. Similar to the previous theoretical studies,[39–41] it can be explained by the electronic reconstruction resulting from the polar discontinuity at the interface.

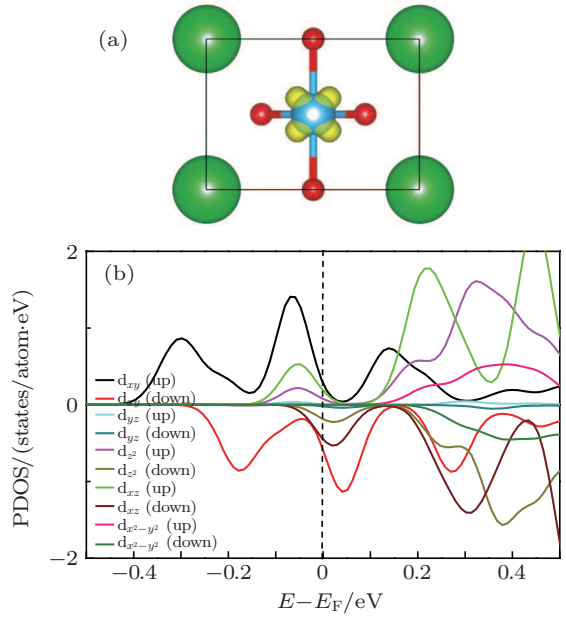


Fig. 3. (color online) (a) The spatial distributions of free electrons (yellow contour) of the interface Ti atom; this is the top view of the interface in Fig. 2(a). (b) The PDOS of the interface Ti 3d states.

To investigate the composition of the interfacial 2DEG, the spatial distributions of free electrons (yellow contour) of the interface Ti atom are shown in Fig. 3(a), which is the top view of the interface in Fig. 2(a). We can see that the 2DEG formed at the interface is dominantly composed of the interface Ti $3d_{xy}$ state, and it can be confirmed by the partial density of states (PDOS) of the interface Ti 3d states, which is shown in Fig. 3(b). From Fig. 3(b), we can see that there is a large splitting of the interface Ti 3d states. This could be explained by the asymmetry at the interface: two O atoms on one side, and two Mg and two O atoms on the other side of the interface Ti atom. The Ti $3d_{xy}$ state splits off from other 3d states by about 0.3 eV. The lowest d_{xy} and higher d_{xz}/d_z^2 orbitals are partly filled, thereby forming a 2DEG. From Fig. 3(b), it can also be seen that there is an unbalance between the spin-up and spin-down states, resulting in a magnetic moment of

about 0.15μ_B on the Ti atom of the interface. Thus the Ti 3d states, especially the lowest d_{xy} state at the interface, contribute greatly to the metallic and magnetic properties of the n-type MgO/BaTiO (110) interface.

The polar $(MgO)^0/(BaTiO)^{4+}$ interface is similar to the $(LaO)^+/(TiO_2)^0$ interface in n-type $LaAlO_3/SrTiO_3$ heterostructures. This polar discontinuity creates an internal electric field in $BaTiO_3$ and thus an increased electric potential across the $BaTiO_3$ layers. It is similar to that which occurred in the $LaAlO_3$ slab of the $LaAlO_3/SrTiO_3$ heterostructure. In the $LaAlO_3/SrTiO_3$ heterostructure, the interface becomes metallic when the $LaAlO_3$ slab thickness is above 4 unit cells.[5,6] Here, we vary the thickness of $BaTiO_3$ to search for the critical thickness of the metallic $BaTiO_3$/MgO (110) interface.

Relaxed 1–4 ML thick $BaTiO_3$ films on MgO (110) are shown in Fig. 4. From the figure, we can see that the relaxation of the MgO slab is unconspicuous in the four models. In contrast, the displacements of atoms in the $BaTiO_3$ slab are significant: Ti and Ba atoms relax away from the interface while O atoms relax close to the interface. It is similar to that in the MgO/BaTiO (110) interface. The total density of states as a function of the $BaTiO_3$ thickness for 1–4 ML thick $BaTiO_3$ films on MgO (110) is shown in Fig. 5(a). With increasing thickness of the $BaTiO_3$ film, the band gap decreases from 1.63 eV for 1 ML $BaTiO_3$ and finally closes for 4 ML BaTiO/MgO (110). The results predict an insulator-to-metal transition. In order to gain more insight into the type of electronic states around the Fermi level and their spatial distribution, the layer-resolved density of states for the 4 ML BaTiO/MgO (110) is calculated, and plotted in Fig. 5(b). From the figure, a nearly rigid upward shift of the O 2p bands towards the Fermi level is observed as they approach the surface. For the relaxed BaTiO/MgO (110) heterostructure, the top of the valence band is determined by the O 2p states in the surface O_2 layer, while the bottom of the conduction band is determined by the Ti 3d states at the interface. Thus, the closing of the gap is due to the raising of the O 2p states in the surface O_2 layer and the reducing of the Ti 3d states at the interface as the $BaTiO_3$ slab gets thicker. Once the $BaTiO_3$ slab thickness is above 4 unit cells, the BaTiO/MgO (110) interface becomes metallic, and a 2DEG is formed at the interface.

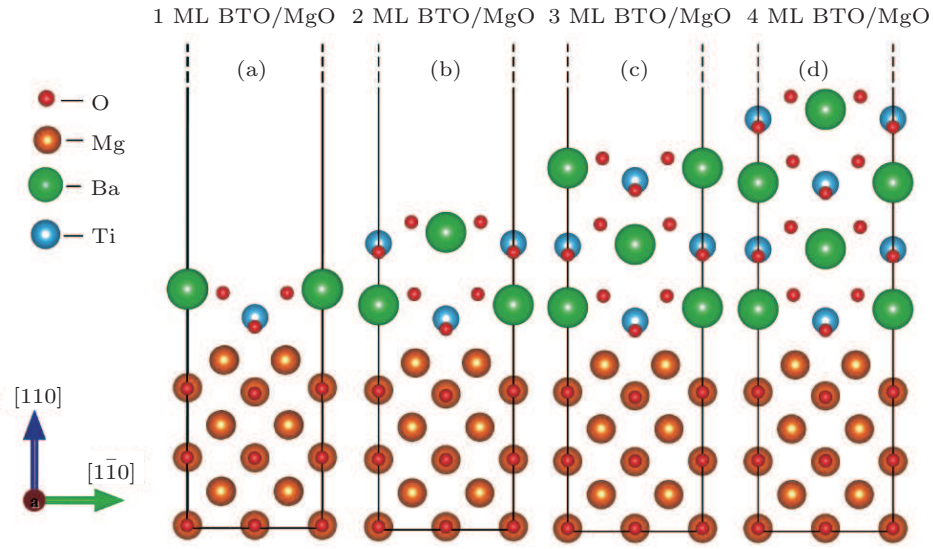


Fig. 4. (color online) Relaxed (a) 1 ML, (b) 2 ML, (c) 3 ML, and (d) 4 ML thick $BaTiO_3$ films on MgO (110).

MgO grown on a $BaTiO_3$ substrate is under compressive stress, while $BaTiO_3$ grown on a MgO substrate is under tensile stress. The different interface stress may influence the formation of the 2DEG. To investigate the composition of the 2DEG formed at the BaTiO/MgO (110) interface, the 3D isovalue surface (yellow contour) of the local density of states of the interface Ti atom for 5 ML BaTiO/MgO (110) is calculated, and shown in Fig. 6(a). From the figure, we can see that the 2DEG formed at the interface is dominantly composed of interface Ti $3d_{xy}$ and $3d_{xz}$ orbitals, and it can be confirmed by the PDOS of the interface Ti 3d states, which is shown in Fig. 6(b). From the figure, we can see that there is a large splitting of the interface Ti 3d states: the Ti $3d_{xy}$ state splits off from other 3d states by about 0.1 eV. The lowest d_{xy} and higher d_{xz}/d_z^2 orbitals are partly filled, thereby forming a 2DEG. In addition, from Fig. 6(b), it can also be seen that there is an unbalance between the spin-up and spin-down states, resulting in a magnetic moment of about 0.20μ_B on the Ti atom of the interface. Comparing Fig. 6 with Fig. 3, it can be found that the occupation and splitting of the interface Ti 3d states are different. It suggests that the interface stress plays an important role in the composition of the 2DEG.

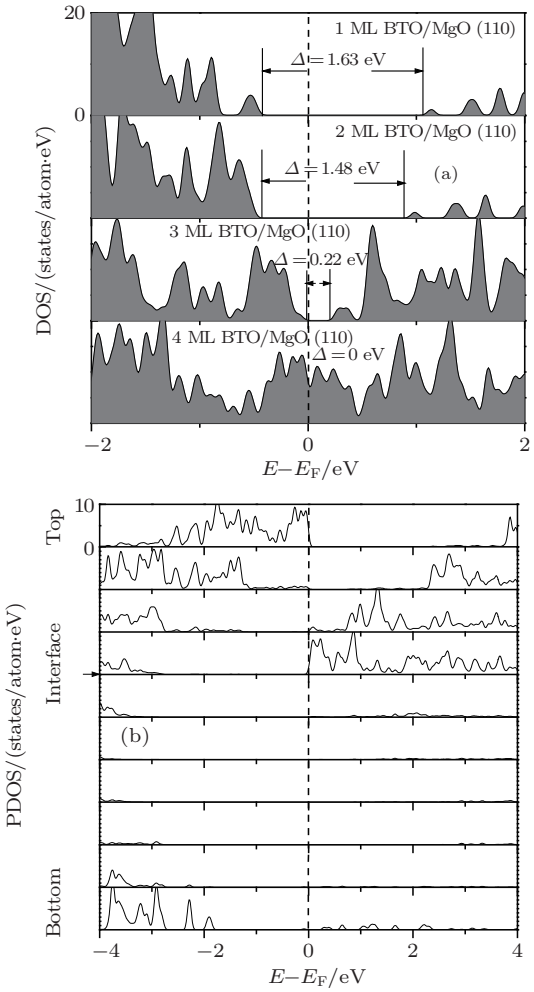


Fig. 5. (a) The total density of states as a function of the $BaTiO_3$ thickness for 1–4 ML thick $BaTiO_3$ films on MgO (110). (b) The layer-resolved density of states for 4 ML BaTiO/MgO (110).

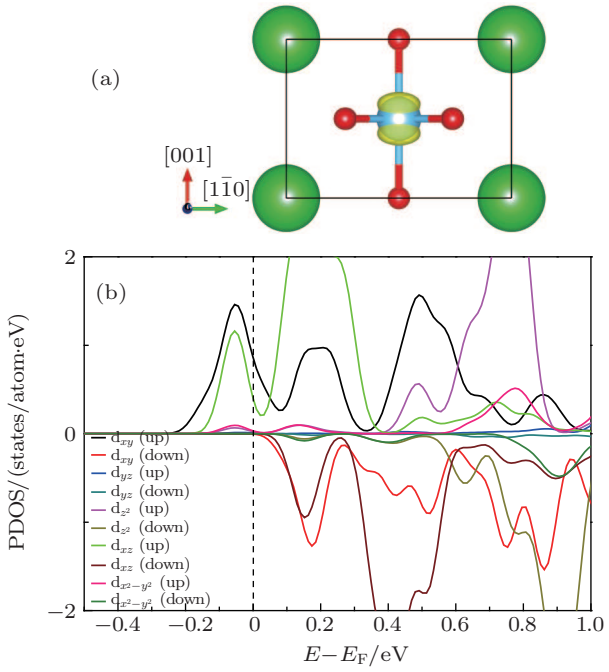


Fig. 6. (color online) (a) The 3D isovalue surface (yellow contour) of the local density of states of the interface Ti atom contributing to the peak at the Fermi level. (b) The partial density of states (PDOS) of the interface Ti 3d states.

3.2. The p-type interface

Figure 7 shows the relaxed p-type MgO/O_2 (110) interface. From the figure, we can see that the relaxation of the $BaTiO_3$ slab is more obvious than that of the MgO slab. In addition, it can be seen that both Ti and Ba atoms relax close to the interface, while all O atoms relax away from the interface. A more thorough insight can be obtained by analyzing the relative displacements between M (M denotes Ba, Ti or Mg) and O atoms, which are listed in Table 2. From the table, we can see that the largest structural relaxation occurs in the interface BaTiO layer. In the layer, the relative displacement between O and Ba atoms results in a big buckling of 0.40 Å. The relative displacement between O and Ti (Ba) ions results in a polarization $\boldsymbol{P}$ pointed to the interface, which can reduce the built-in potential in the $BaTiO_3$ (110) slab and the instability of the polar interface.

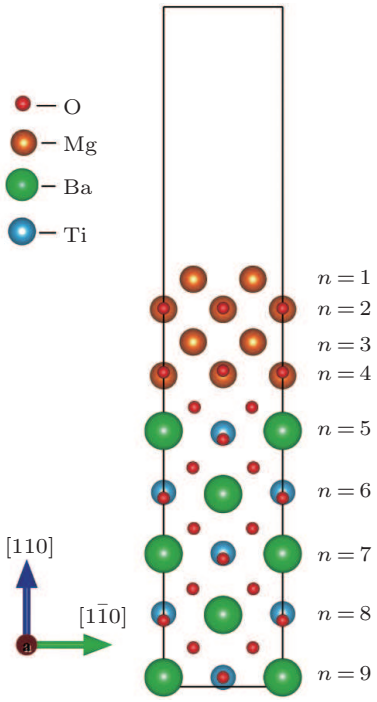


Fig. 7. (color online) Relaxed structure of the $(MgO)_8/(BaTiO_3)_5$ (110) heterostructure with a p-type $(MgO)^0/(O_2)^{4-}$ interface, containing 8 unit cells (four layers) of MgO and 5 unit cells of $BaTiO_3$ within the heterostructure. Index n denotes atomic monolayers and is increasing with the distance from the surface.

Figure 8 displays the electronic properties of the p-type MgO/O_2 (110) interface. Figure 8(a) shows the 3D isovalue surface (yellow contour) of the local density of states contributing to the peak at the Fermi level, which describes the spatial distribution of transferred electrons and holes. From the figure, it can be observed that the electrons are confined in the bottom layer, while the holes are confined at the interface MgO layer. In order to gain more insight into the spatial distribution of electronic states, the partial density of states grouped by layers of the heterostructure is shown in Fig. 8(b). Owing

to the polar structure of $BaTiO_3$ along the [110] direction, the electric field through the $BaTiO_3$ film lifts up the valence band edge and reduces the band gap. When the interface O $2p_y$ state surpasses the Fermi level, a conducting interface emerges. It can also be explained by the electronic reconstruction resulting from the polar discontinuity at the interface.

Table 2. Relative displacements between relaxed M (M denotes Ba, Ti or Mg) and O atoms $\Delta(M\text{–O})$. The relative displacement denotes the displacement of cations (Ba, Ti or Mg) minus that of O anions in each layer along the c axis.

Layer n	1	2	3	4	5	6	7	8	9
Δ(Ba–O)/Å	–	–	–	–	0.40	0.18	0.23	0.27	0.00
Δ(Ti–O)/Å	–	–	–	–	0.29	0.26	0.26	0.30	0.00
Δ(Mg–O)/Å	–0.10	–0.06	–0.06	–0.16	–	–	–	–	–

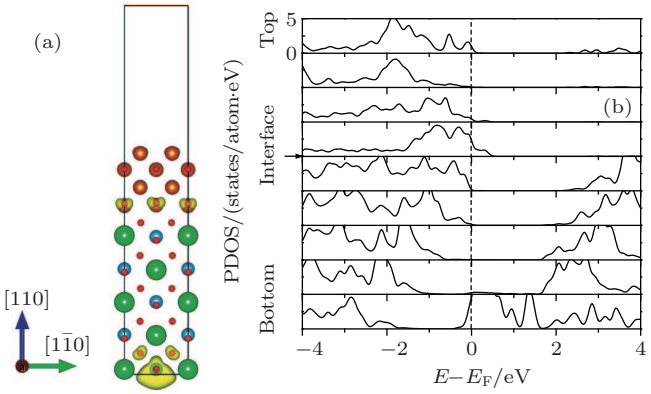


Fig. 8. (color online) (a) The 3D isovalue surface (yellow contour) of the local density of states contributing to the peak at the Fermi level. (b) The partial density of states grouped by layers of the $(MgO)_8/(BaTiO_3)_5$ (110) heterostructure with a p-type interface. The data (plot of a charge isosurface and PDOS) for each layer are aligned on the same vertical position. The Fermi level is highlighted by the black dashed line.

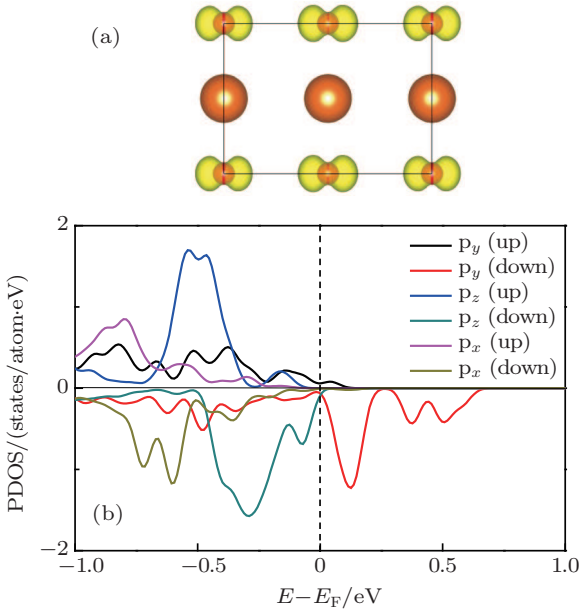


Fig. 9. (color online) (a) The 3D isovalue surface (yellow contour) of the local density of states of the interface MgO layer contributing to the peak at the Fermi level, and it is the top view of the interface in Fig. 8(a). (b) The PDOS of the O 2p states in the interface MgO layer.

To investigate the composition of the interfacial holes, the 3D isovalue surface (yellow contour) of the local density of states of the interface MgO layer contributing to the peak at the Fermi level is calculated, and shown in Fig. 9(a). From the figure, we can see that the interfacial holes dominantly come from the O $2p_y$ orbital in the interfacial MgO layer, and it can be confirmed by the PDOS of the O atoms in the interfacial MgO layer shown in Fig. 9(b). In Fig. 9(b), we can see that the interface O 2p states split and the O $2p_y$ state splits off from other O 2p states by 0.55 eV. The partly filled O $2p_y$ state contributes mainly to the formation of the interface holes. In addition, there is an unbalance between the spin-up and spin-down states, resulting in a magnetic moment of about $0.25\mu_B$ on the O atom of the interface.

4. Conclusion

The results of first-principles calculations clearly demonstrate that other polar interfaces, besides $LaAlO_3/SrTiO_3$, can show a two-dimensional metallic behavior. Based on the analyses of the electronic properties of the n-type polar interfaces, it can be seen that the interface Ti 3d states contribute greatly to the metallic and magnetic properties. Varying the thickness of $BaTiO_3$ may induce a metal–insulator transition. Once the $BaTiO_3$ slab thickness is above 4 unit cells, the n-type interface becomes metallic. For the p-type polar interface, holes preferentially occupy the interface O $2p_y$ state, resulting in a conducting interface. The unbalance of the spin splitting of the O 2p states in the interface MgO layer leads to a magnetic moment of about $0.25\mu_B$ per O atom at the interface. All these results add to the understanding of these polar interfaces and further suggest that interface engineering is an attractive and useful approach to creating novel properties in correlated electron systems.

References

[1] Ohtomo A and Hwang H Y 2004 *Nature* **427** 423
[2] Kalabukhov A, Gunnarsson R, Börjesson J, Olsson E, Claeson T and Winkler D 2007 *Phys. Rev. B* **75** 121404
[3] Siemons W, Koster G, Yamamoto H, Harrison W A, Lucovsky G, Geballe T H, Blank D H A and Beasley M R 2007 *Phys. Rev. Lett.* **98** 196802
[4] Maurice J L, Herranz G, Colliex C, Devos I, Carrétéro C, Barthélémy A, Bouzehouane K, Fusil S, Imhoff D, Jacquet E, Jomard F, Ballutaud D and Basletic M 2008 *Europhys. Lett.* **82** 17003
[5] Huijben M, Rijnders G, Blank D H A, Bals S, Aert S V, Verbeeck J, Tendeloo G V, Brinkman A and Hilgenkamp H 2006 *Nat. Mater.* **5** 556

[6] Bell C, Harashima S, Hikita Y and Hwang H Y 2009 *Appl. Phys. Lett.* **94** 222111
[7] Thiel S, Hammerl G, Schmehl A, Schneider C W and Mannhart J 2006 *Science* **313** 942
[8] Caviglia A D, Gariglio S, Reyren N, Jaccard D, Schneider T, Gabay M, Thiel S, Hammerl G, Mannhart J and Triscone J M 2008 *Nature* **456** 624
[9] Yang X P and Su H B 2011 *ACS Appl. Mater. Interfaces* **3** 3819
[10] Bark C W, Felker D A, Wang Y, Zhang Y, Jang H W, Folkman C M, Park J W, Baek S H, Zhou H, Fong D D, Pan X Q, Tsymbal E Y, Rzchowski M S and Eom C B 2011 *Proceedings of the National Academy of Sciences* **108** 4720
[11] Pentcheva R and Pickett W E 2006 *Phys. Rev. B* **74** 035112
[12] Park M S, Rhim S H and Freeman A J 2006 *Phys. Rev. B* **74** 205416
[13] Verbeeck J, Bals S, Kravtsova A N, Lamoen D, Luysberg M, Huijben M, Rijnders G, Brinkman A, Hilgenkamp H, Blank D H A and Tendeloo G V 2010 *Phys. Rev. B* **81** 085113
[14] Wang H Y, Duan Z G, Liao W H and Zhou G H 2010 *Chin. Phys. B* **19** 037301
[15] Du Y L, Wang C L, Li J C, Xu P P, Zhang X H, Liu J, Su W B and Mei L M 2014 *Chin. Phys. B* **23** 087302
[16] Nakagawa N, Hwang H Y and Muller D 2006 *Nat. Mater.* **5** 204
[17] Hotta Y, Susaki T and Hwang H Y 2007 *Phys. Rev. Lett.* **99** 236805
[18] Wang Y, Niranjan M K, Burton J D, An J M, Belashchenko K D and Tsymbal E Y 2009 *Phys. Rev. B* **79** 212408
[19] Perna P, Maccariello D, Radovic M, Scotti di Uccio U, Pallecchi I, Codda M, Marré D, Cantoni C, Gazquez J, Varela M, Pennycook S J and Granozio F M 2010 *Appl. Phys. Lett.* **97** 152111
[20] Aboelfotoh M O 1975 *Journal of Vacuum Science and Technology* **12** 67
[21] Geguzina G A and Sakhnenko V P 2004 *Crystallography Reports* **49** 15
[22] Murphy T E, Chen D and Phillips J D 2004 *Appl. Phys. Lett.* **85** 3208
[23] Petraru A, Schubert J, Schmid M and Buchal Ch 2002 *Appl. Phys. Lett.* **81** 1375
[24] Buchal Ch, Beckers L, Eckau A, Schubert J and Zander W 1998 *Mater. Sci. Engng B* **56** 234
[25] Kim S, Hishita S, Kang Y M and Baik S 1995 *J. Appl. Phys.* **78** 5604
[26] Shih W C, Chiang M H and Mater J 2010 *Sci.: Mater Electron.* **21** 844
[27] Zhang W Kang L M, Yuan M L, Yang Q and Ouyang J 2013 *J. Alloy. Compd.* **580** 363
[28] Towner D J, Ni J, Marks T J and Wessels B W 2003 *J. Cryst. Growth* **255** 107
[29] Hiltunen J, Seneviratne D, Tuller H L, Lappalainen J and Lantto V 2009 *J. Electroceram* **22** 395
[30] Wu Z, Cohen R E and Singh D J 2004 *Phys. Rev. B* **70** 104112
[31] Bilc I, Orlando R, Shaltaf R, Rignanese G M, Íñiguez Jorge and Ghosez Ph 2008 *Phys. Rev. B* **77** 165107
[32] Wei X H, Zhu J and Li Y R 2011 *Vacuum* **85** 999
[33] Kresse G and Furthmüller J 1996 *Phys. Rev. B* **54** 11169
[34] Kresse G and Joubert D 1999 *Phys. Rev. B* **59** 1758
[35] Blöchl P E 1994 *Phys. Rev. B* **50** 17953
[36] Ceperley D M and Alder B J 1980 *Phys. Rev. Lett.* **45** 566
[37] Monkhorst H J and Pack J D 1976 *Phys. Rev. B* **13** 5188
[38] Sivadas N, Dixit H, Cooper V R and Xiao D 2014 *Phys. Rev. B* **89** 075303
[39] Willmott P R, Pauli S A, Herger R, Schlepütz C M, Martoccia D, Patterson B D, Delley B, Clarke R, Kumah D, Cionca C and Yacoby Y 2007 *Phys. Rev. Lett.* **99** 155502
[40] Lee J, Sai N and Demkov A A 2010 *Phys. Rev. B* **82** 235305
[41] Pentcheva R and Pickett W E 2009 *Phys. Rev. Lett.* **102** 107602